Environmental Earth Sciences (2018) 77:77
https://doi.org/10.1007/s12665-018-7252-6

ORIGINAL ARTICLE

Spatiotemporal monitoring of land surface temperature and estimated radiation using remote sensing: human health implications for East London, South Africa

I. R. Orimoloye[1] · S. P. Mazinyo[1] · W. Nel[1] · A. M. Kalumba[1]

Received: 1 September 2017 / Accepted: 12 January 2018 / Published online: 24 January 2018

Abstract
Increase in land surface temperature (LST) and area radiation (*R*) has serious health implications on human life. Therefore, investigating LST and *R* changes is fundamental in providing crucial information for human survival. Remote sensing was used to assess the LST and estimated radiation of East London city in Eastern Cape Province of South Africa from Landsat thematic mapper images for 1986, 1996, 2006, and operational land imager, thermal infrared sensor for 2016 spanning a period of 30 years. Rapid urbanization and land cover changes in this area have contributed significantly to this drastic change in the natural surface characteristics (increased land surface temperature and surface solar radiation). For instance, vegetation cover declined by about 358.812 km^2 and built-up increased built-up area by 175.473 km^2 during this period, which correlates with the area thermal characteristics changes. Also, the radiation increased over the years with values exceeding the global solar radiation index. Exposure to increased ultraviolet radiation possesses risks of heat stroke, skin cancer, and heart disease to the local population. Consequently, this study provides pertinent information for human health sustainability and epidemiological cases management. Further investigation is needed in established case-specific causes. This study also epitomises the significance of remote sensing climate variability studies.

Keywords Land surface temperature · Radiation · Human health · Remote sensing · Exposure

Introduction

Land use and land cover changes modify the local and regional climates with tremendous effects on the LST and area radiation. Literature has shown that changes in LST and area radiation increase with changes in land cover, especially in urban areas (Ige et al. 2017). Numerous authors have also noted that there are serious health implications of an increase in LST and area radiation (Tursilowati and Djundjunan 2007; Weng et al. 2004; Peng et al. 2014). These health impacts have been registered in different forms such as global solar radiation index threshold, temperature relative index, thermal comfort index, discomfort index (WHO 2003; Tursilowati and Djundjunan 2007; Xu et al. 2017). To this end, there is a need for constant monitoring changes in LST and area radiation as per the global solar radiation index, especially in the urban context. This could help to design appropriate mitigation and adaptation strategies.

Urbanization through the development of urban societies and rural regions has resulted in climatic modification (Tursilowati and Djundjunan 2007; Peng et al. 2014) and land cover changes. Remote sensing and GIS techniques have been widely used in monitoring urban growth and in detecting the changes that have occurred and its associated environmental injustice in the urban areas (Adeola et al. 2017; Stephen et al. 2017; Adefisan et al. 2015; Ige et al. 2017; Onamuti et al. 2017). Land covers as biophysical (environment) condition of earth's surface and direct subsurface are sources and sinks for the most of the materials and energy movements, connections between the biosphere and geosphere. Changes in land cover incorporate urban climate alteration, changes in biotic grouped qualities, genuine and potential required power, soil quality, runoff, and sedimentation rate (Mahmood et al. 2014; IPCC 2014), and all these cannot be completely comprehended without the data or idea of land features used that influence them. Moreover,

✉ I. R. Orimoloye
orimoloyeisrael@gmail.com

[1] Department of Geography and Environmental Science, University of Fort Hare, Alice 5700, South Africa

land use land changes (LULC) have ecological indications at local and regional levels as this might be connected to the global climate and natural process. In the light of this associated nature of the parts of the indigenous or natural environment, the immediate impacts of one segment may bring about indirect effects on others. Urban microclimates have been recognized for more than 100 years ago (Howard 1833) later by Oke (1978), and in the monitoring and recognition of global climate change, climate experts have done great jobs to minimize or manage the potential influence of urbanization on the chronicled climate records (Parker 2010; Ropo et al. 2017).

LST, which can alter or modify air temperature of a layer of the lower air or atmosphere, has been investigated in the previous studies using remotely sensed information such as Landsat imageries including thematic mapper (TM), enhanced thematic mapper (ETM), operational land imager (OLI), and thermal infrared sensor (TIRS) (Ige et al. 2017; Xu et al. 2017). This study used TM for year 1986, 1996, 2006 and OLI and TIRS for year 2016 to estimate the thermal characteristics of the study area.

This study focused on the surface land temperature, land surface solar radiation. In so doing, the study aimed at estimating land surface thermal characteristics using Landsat images with high resolution, to quantify the spatial configuration of LST and radiation in the study area and examine the connections between land use and the thermal signal at different years spanning 30 years (1986–2016).

Study area

East London lies on the southeast coast of South Africa in the Buffalo City Metropolitan Municipality (BCMM), Eastern Cape Province. The area is found at Latitude 32°59′0″S and Longitude 27°52′0″E. with an area of about 21,043 km^2 (979 sq. miles). East London has a humid subtropical climate with the warm temperatures (Fitchett et al. 2017) and has an all-time lowest temperature of 3 °C (37.4 °F) and all-time highest temperature records of 42 °C (107.6 °F) (Fig. 1).

Materials and methods

Image preprocessing

The 1986, 1996, 2006 thematic mapper (TM) and 2016 operational land imager (OLI), thermal infrared sensor (TIRS) Landsat eight imageries were obtained from the US Geological Survey archive and were registered to 1:150.000 shapefile maps of East London area. Each image was radiometrically corrected as stated in Chander and Markham (2003) (Table 1).

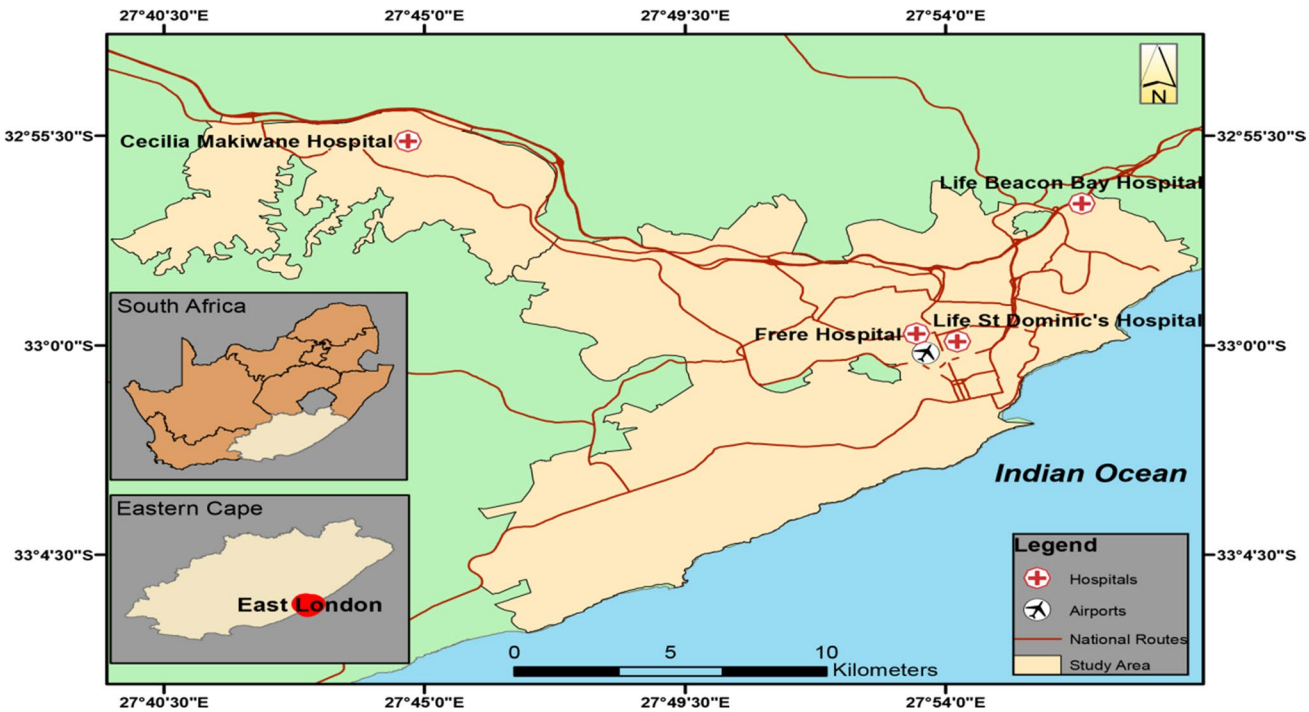

Fig. 1 East London area in Buffalo city metropolitan municipality, South Africa

Table 1 Specification of data used

Data	Year	Date acquired	Path/row	Thermal lines
Landsat thematic mapper (Landsat 5 TM)	1986	1986-12-12	169/083	7111
Landsat 5 TM	1996	1996-02-09	169/083	7201
Landsat 5 TM	2006	2006-02-04	169/083	7161
Landsat 8 OLI_TIRS	2016	2016-12-10	169/083	7891

Image classification

In this study, all raw images of East London area were acquired from the archives of US Geological Survey (USGS). The imageries collected for the analysis are in four components, image data in 1986, 1996, 2006, and 2016 all have good quality with less 10% cloud cover in the selected area. The information in Table 2 shows the specifications of the image of the East London used for this study, and the images are named after their imaging time by month, year and day of the year incorporated with path and row, and thermal lines of different imageries were analyzed using ArcGIS 10.2. The operational land imager (OLI) image comprises of the near-infrared (NIR) band, shortwave infrared (SWIR) band, visible bands, and thermal infrared (TIR) band, which are present in TM images (1986, 1996, 2006 images). TIRS bands are also thermal infrared bands with a higher resolution compared with TIR bands (2016 image).

Land cover classes are typically mapped from digital remotely sensed data through the process of a supervised digital image classification (Tewkesbury et al. 2015; Liu and Yang 2015; Shalaby and Tateishi 2007). The goal of the image classification process is to automatically categorize all pixels in an image into land cover classes (Shalaby and Tateishi 2007). The maximum likelihood classifier quantitatively evaluates both the variance and covariance of the category spectral response patterns when classifying an unknown pixel so that it is considered to be one of the most accurate classifiers since it is based on statistical parameters. This study used supervised classification and using ground checkpoints with digital topographic maps of the East London area. The area was classified into five main classes: built-up, vegetation, open surface, water body, and beaches. Descriptions of these land cover classes are presented in Table 3.

Table 3 Supervised classification of land features and its percentage between 1986 and 2016

Various land use/land cover identified	Area coverage (km^2)	Percentage coverage (%)
1986		
Built-up area	(609.912)	(28)
Water body	(18.441)	(1)
Vegetation	(1029.204)	(48)
Open surface	(472.752)	(22)
Beaches	(12.132)	(1)
1996		
Built-up area	(708.192)	(33)
Water body	(13.554)	(1)
Vegetation	(664.11)	31
Open surface	(734.544)	34
Beaches	(22.041)	(1)
2006		
Built-up area	(784.296)	36
Water body	(14.967)	1
Vegetation	(791.802)	37
Open surface	(536.589)	25
Beaches	(14.787)	1
2016		
Built-up area	(785.385)	37
Water body	(19.962)	1
Vegetation	(670.392)	31
Open surface	(652.752)	30
Beaches	(13.95)	1

Estimation of land surface temperature

LST was obtained from the balanced or adjusted TM (1986, 1996, 2006, and 2016) by employing the technique used in Chander and Markham (2003), which does not require climatic variables and is utilized generally. And, the digital numbers were changed into radiance using the equation below:

$$R\lambda = \left(\frac{\text{RMAX} - \text{RMIN}}{\text{QCALMAX} - \text{QCALMIN}}\right) \times (\text{Thermal Band} - \text{QCALMIN}) + \text{LMIN},$$

where R_{λ}, Spectral Radiance at the sensor's opening in watts/(meter squared * steradian * μm); QCAL, the quantized adjusted pixel value in DN; RMINλ, the spectral radiance that is scaled to QCALMIN in watts/(meter

Table 2 Value for estimation of radiance temperature. (*Source*: Williams 2009)

	LMAX	LMIN	QCALMAX	QCALMIN	K_1	K_2
Landsat 5	15.303	1.238	255	1	1260.56	607.76
Landsat 8	89.58701	− 7.39812	65535	1	744.89	1321.08

squared * ster * μm); RMAXλ, the spectral radiance that is scaled to QCALMAX in watts/(meter squared * ster * μm); QCALMIN, the base quantized adjusted pixel value; relating to LMINλ) in DN; QCALMAX, the highest quantized adjusted pixel value (comparing to LMAXλ) in DN.

The change of the spectral radiance into a satellite brightness temperature (*Tb*) under the supposition of uniform emissivity utilizes the following algorithm:

$$T_{\mathrm{b}} = \frac{K_2}{\ln\left(\frac{K_1}{R_\lambda} + 1\right)},$$

where *Tb* is the efficient satellite temperature in Kelvin, R_λ is the spectral radiance at the sensor's space, and K_1 *and* K_2 are the calibration constants 607.76 and 1260.56 mW/(cm^2 sr ŋm), respectively. The outcome of this process or the values is therefore referenced to black body. In the process of estimating the land surface temperature, the emissivity corrected land surface temperatures were analyzed in line with Williams (2009) and Weng et al. (2004).

$$\text{Land surface temperature} = \frac{T_b}{1 + \left(\lambda \times T_b(\rho)\ln\varepsilon\right)},$$

where $\lambda = 11.5$ mm, $\rho = 1.438 \times 10^{-2}$ mk, and ε is the land emissivity, which was calculated using normalized difference vegetation index (NDVI) threshold technique (Chander and Markham (2003), and the threshold is as follows;

$\varepsilon = \varepsilon_{\mathrm{soil}}$ when NDVI < 0.2; $\varepsilon = \varepsilon_{\mathrm{vegetation}}$ when NDVI > 0.5, therefore,

$\varepsilon = \varepsilon_{\mathrm{vegetation}} P_{\mathrm{v}+} \varepsilon_{\mathrm{soil}} (1 - P_v)$

When $0.2 \leq \mathrm{NDVI} \leq 0.5$ where $\varepsilon_{\mathrm{soil}}$ is the emissivity of soil, $\varepsilon_{\mathrm{vegetation}}$ is the vegetation emissivity, and P_v is the vegetative proportion calculated from the method of Carlson and Ripley (1997),

$$P_{\mathrm{v}} = \left(\left(\mathrm{NDVI} - \mathrm{NDVI}_{\mathrm{min}}\right)/\left(\mathrm{NDVI}_{\mathrm{max}} - \mathrm{NDVI}_{\mathrm{min}}\right)\right)^2$$

Therefore, vegetation and soil emissivity were obtained.

NDVI was obtained from the pixel values of the Landsat TM as:

$$\mathrm{NDVI} = \frac{\mathrm{float}((B4) - (B3))}{\mathrm{float}((B4) + (B3))},$$

where *B*3 and *B*4 are band 3 and band 4 for Landsat 5, respectively, and B4 and B3 were substituted with *B*5 and *B*4 in Landsat 8, respectively.

Estimation of surface radiation

Thermal radiation is energy exchange by the discharge or reflection of electromagnetic waves that transport energy from the emanating or reflecting object. In retrieving radiation power from the satellite imageries, this study employed Stefan-Boltzmann law and the methods used by Chander and Markham (2003), which helps to resolve the unknown quantity between radiations emitted by the surface. This method outlines the energy transmitted by the body radiator every second per unit area is relative to the power of the total temperature emanated from the surface regarding its temperature. Below is the equation:

$$P = \varepsilon\sigma A T^4,$$

where *P*, Radiation power; ε, emissivity; σ, Stefan's constant (0.000000567 Wm^{-2}); *T*, Temperature (land surface temperature); *A*, surface area = $4\pi r^2$.

r is derived from the angle subtended by an arc of a circle equal in length to the radius of the circle: 57.3° (Roy et al. 2016) and converted to meter which is also equivalent to the radius of the earth, 6371 km, and π is a scientific constant, the proportion of a circle's circumference to its measurement, ordinarily approximated as 3.14159. It has been represented by the Greek letter "π" since the mid-eighteenth century; however, it is likewise spelled out as "**pi.**"

Result and discussion

Land features characteristics of East London image classification between 1986 and 2016

The analysis of supervised classification of the study area between 1986 and 2016 is shown in Fig. 2; and also along with the land area coverage for the various land features retrieved from the imagery presented in Table 3, the area covered with different land features (built-up, vegetation, water body, open surface (dead or stressed vegetation, bare surface, new cultivated area, sand fill, and rock), and beaches) vegetation cover in year 1986 was (1029.204) km^2 followed by built-up area of about (609.912) km^2; the area covered by water body was (18.441) km^2 while open surface and beaches cover (472.752) and (12.132) km^2, respectively.

More so, the results revealed that there was a drastic change (Table 3) in vegetation cover between 1986 and 1996; built-up area and vegetation cover an area of (708.192) and (664.11) km^2, respectively, while water body is (13.554) km^2 lesser than the last decade with about (4.887) km^2. Open surfaces have the highest area coverage for the year 1996 with about (734.544) km^2 and beaches with (22.041) km^2. Land features characteristics for 2006 as presented in Fig. 2 and Table 3 with the percentage of the area covered for each feature include built-up, vegetation, open surface, water body, and beaches for the year 2006. Vegetation covers land area of about (791.802) km^2

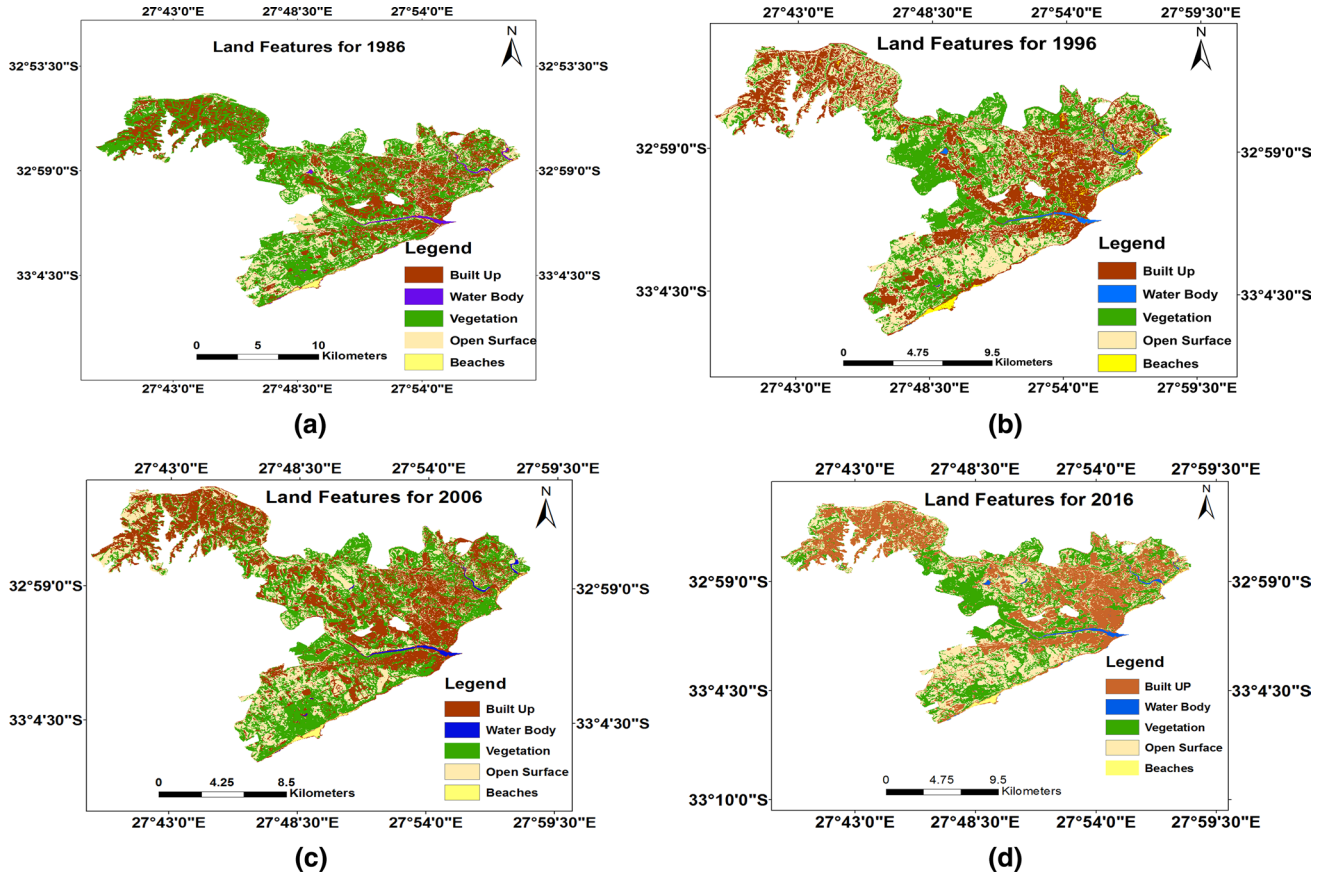

Fig. 2 Land use features between 1986 and 2016. **a** 1986, **b** 1996, **c** 2006, and **d** 2016

followed by built-up area with (784.296) km^2 for year 2006. While water body and open surface have area coverage of (14.967) and (536.589) km^2 respectively, for the current year, beaches have area coverage of (14.787) km^2. In year 2016, vegetation in the area decreased drastically compare with the previous decades where built-up and vegetation area coverage of (785.385) and (670.392) km^2 respectively. Water body covers land area of about (19.962) km^2 while open surface and beaches have land cover of (652.752) and (13.95) km^2, respectively, for the same year.

Results from the analysis revealed that the study area has experienced changes in the past 3 decades, and the land use features accuracy assessment of the land use/cover classification results obtained showed an overall accuracy of 76.13%.

Figure 2 and Table 3 depict spatial distributional trend of land use features during the study period. In the year 1986, the results show that vegetation has the highest percentage of (48%) with coverage of (1029.204) km^2 followed by built-up area with (28)% ((609.912) km^2). Area covered with beaches has the lowest percentage of about (1)% with (12.132) km^2 while water body and open surface have the percentage of (1) and (22)% with (18.441) and (472.752) km^2 land cover, respectively (Table 3). The changes in these natural landscapes of the study area can be attributed to the recent development and urbanization rate in the area (Han et al. 2017; Pan et al. 2016).

The land features and its percentage for 1996 revealed that open surface has the highest land area coverage of about (734.544) km^2 compared to the built-up and vegetation cover with (708.192) and (664.11) km^2, respectively. The high percentage of the open surface and changes in green vegetation in the year 1996 may be as a result of anthropogenic activities including urbanization, deforestation, and bush burning (Kamusoko 2017; Dai et al. 2017; Wang et al. 2017a, b) and shake-up and deregulation and land reform after post-apartheid in 1994 (Mather and Greenberg 2003; Hall 2004, 2007; Lahiff and Cousins 2005), while water body cover area declined with about (4.887) km^2 from the previous decade and beach coverage increased with about (9.909) km^2 compared with the previous decade.

The analysis of land features in the year 2006 (Fig. 2 and Table 3) revealed different land features coverage pattern for the year. The result shows that built-up and vegetation

cover (784.296) and (791.802) km^2 with the percentage of 36 and 37%, respectively. The area covered with beaches has the lowest area coverage with about (14.787) km^2 and water body with (14.967) km^2 for 2006 land feature supervised classification. Current land features of East London (2016) with area coverage percentage show that there is drastic increase in the built-up area with (785.385) km^2, and it was also revealed that the year 2016 had the highest built-up area coverage for the period of study as a result of rapid urbanization experienced in the area, which might be contributed to the urban warming in the area (Kruger and Shongwe 2004; Conlon et al. 2016; Hu et al. 2017). Vegetation covers area of (670.392) km^2 with 31% while the area covered with water body was (19.962) km^2. Open surface and beaches occupy area of (652.752) and (13.95) km^2, respectively (Fig. 2 and Table 3).

There was a drastic change in the land features in the study area between 1986 and 2016 as presented in Fig. 3. The built-up area has undergone an increment of about (175.473) km^2 while vegetation in per contra experiences decrease of about (358.812) km^2 during the study period (Fig. 3). Open surface also increased in this period with (180) km^2 cover area.

Spatial characteristics of land surface temperature and its potential impact on human health of the study area between 1986 and 2016

Land surface temperature of East London is presented in Fig. 4a–d; each year has its thermal signal and it was depicted from the analysis that the LST was higher in the built-up region compared to the regions covered with vegetation and other land features.

The result shows that there was variation in LST between 1986 and 2016, and it was also revealed that the built-up area connotes that the urban area has high thermal signal as shown in Fig. 4a–d compared with the other land features that have a lower land surface temperature probably due to vegetation cover and water body as stated by Peng et al. (2014), which implies deforestation can modify surface thermal signal characteristics (Piao et al. 2015; Zhou et al. 2015; Wang et al. 2017a, b; Hu et al. 2017; Conlon et al. 2016). In the year 1994, the spatial distribution of LST was evident and also revealed that the LST in most parts of the study area is above 25 °C and this corroborates with the supervised classification of land features of the study in Fig. 2 that have the highest land cover area of open surface with (734.544) km^2 and the highest percentage of the year with 34% (Table 3), which may cause the increase in land surface temperature (Peng et al. 2014; Wang et al. 2017a, 2017b; Hu et al. 2017; Wang et al. 2016). These changes have constrained the development of urban heat impact at both the urban cover and boundary layers as well as an addition to expansion in ground-level ozone creation which might have a significant impact on human health (Lo and Quattrochi 2003; Conlon et al. 2016).

In 2016, the result revealed that LST increase from the outskirt of the built-up region to the inner city also makes the city warmer than the surrounding areas (Streutker 2003). Studies have shown that the increased temperature has been identified to be associated with heat-related illnesses with prolonged exposure and possible death among the aged and the minor especially in individuals with existing disease as these can make their health condition worsen with increased urban heat (Wilker et al. 2012; Das et al. 2014, Ropo et al. 2017). Consequently, as the urban areas continue to grow, there is tendency or probability of the city area to get warmer

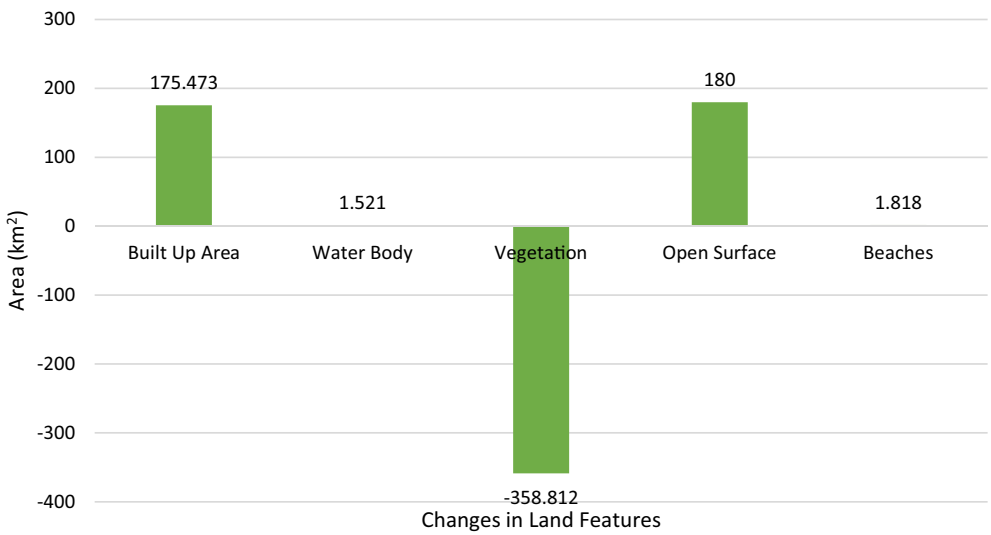

Fig. 3 Diagrammatic illustration of land feature changes in kilometers during the last 3 decades (1986–2016) in the East London

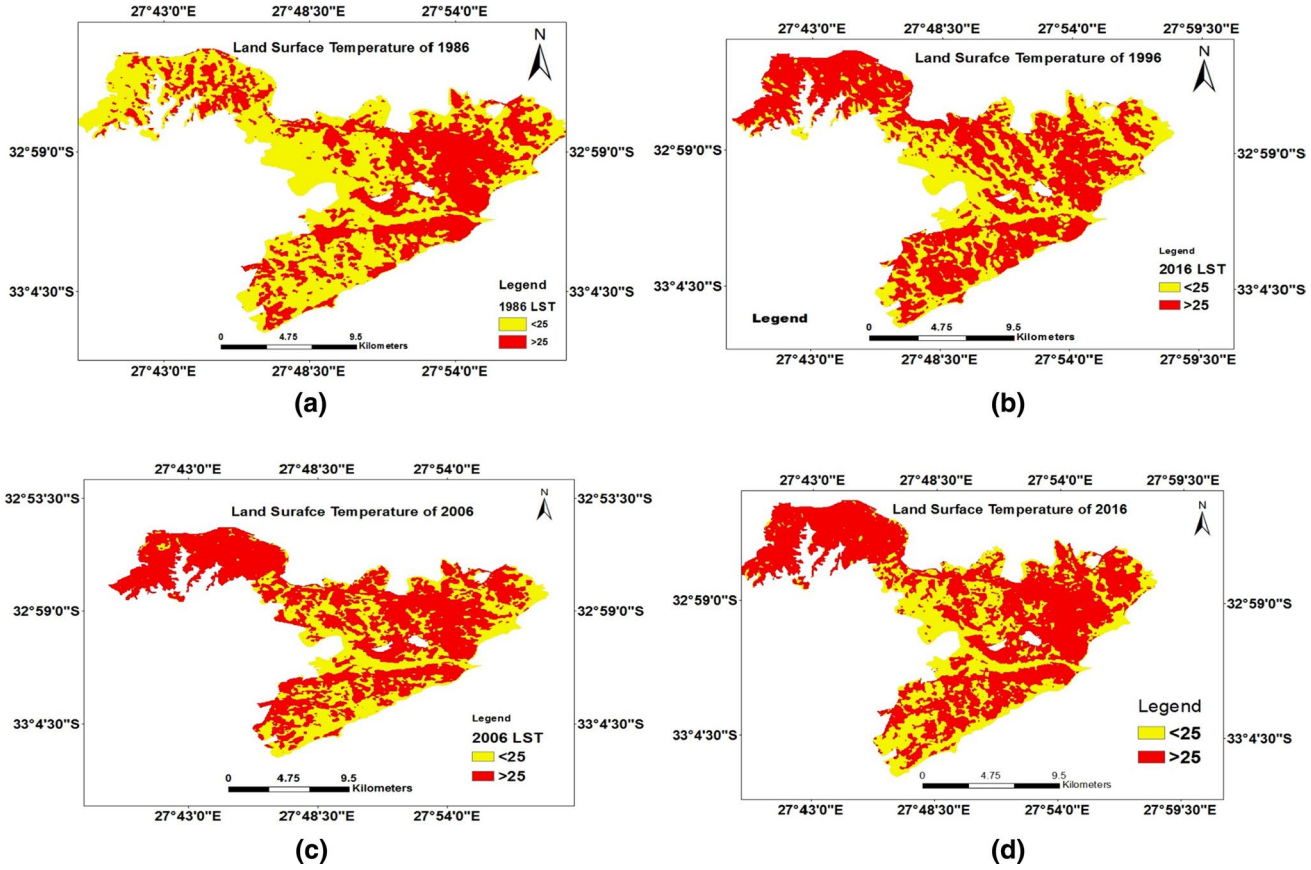

Fig. 4 Land surface temperature of east London between 1986 and 2016; **a** 1986, **b** 1996, **c** 2006, and **d** 2016

than the surrounding suburb due to the increased surface temperature in the area, and these developments can lead to health threat among the dwellers of East London (Bind et al. 2014; Wichmann et al. 2011).

Spatial pattern of estimated radiation and health implications of the study area between 1986 and 2016

The analysis of solar radiation of East London is presented in Fig. 5a–d. These were estimated using the method of Boltzmann law incorporated with the methods used by Chander and Markham (2003) and Landsat 7 Science Data Users Handbook to retrieve solar radiation from the satellite images.

Sunlight, a basic essential for life, might be extremely risky or harmful to human well-being. Too much exposure to the sun is known to be related to increased vulnerability to a various forms of illnesses such as skin malignancies, cataracts, and other diseases, and additionally quickened skin maturing. It might additionally unfavorably influence individuals' capacity to oppose infectious disease (Balk 2011). In the year 1995, global solar radiation index was developed by WHO and later recommended by the International Commission on Non-Ionizing Radiation Protection (ICNIRP), World Meteorological Organization (WMO), and the United Nations Environment Programme (UNEP). Repacholi (2000) used global radiation index to investigate potential human health implication of ultraviolet solar radiation, the index is portrayed, and it is suggested that generally common messages ought to be related to the threshold of the index for a reliable appraisal of solar radiation impacts on human health (Ropo et al. 2017).

Figure 5a–d presents the surface solar radiation pattern between 1986 and 2016 of East London, and it was revealed that in the year 2016, the surface solar radiation was above 10, which was signified as extreme by the WHO (2003) as shown in Table 4 followed by 2006 which fell around the same ranges.

The global solar ultraviolet index is a suitable tool developed through the work of the WHO INTERSUN projected to help the general public and health experts in giving direction or guidance on the level of protection to be used on any given day. It gives a scope of the most extreme solar radiation exposure at the earth's surface. While the intensity

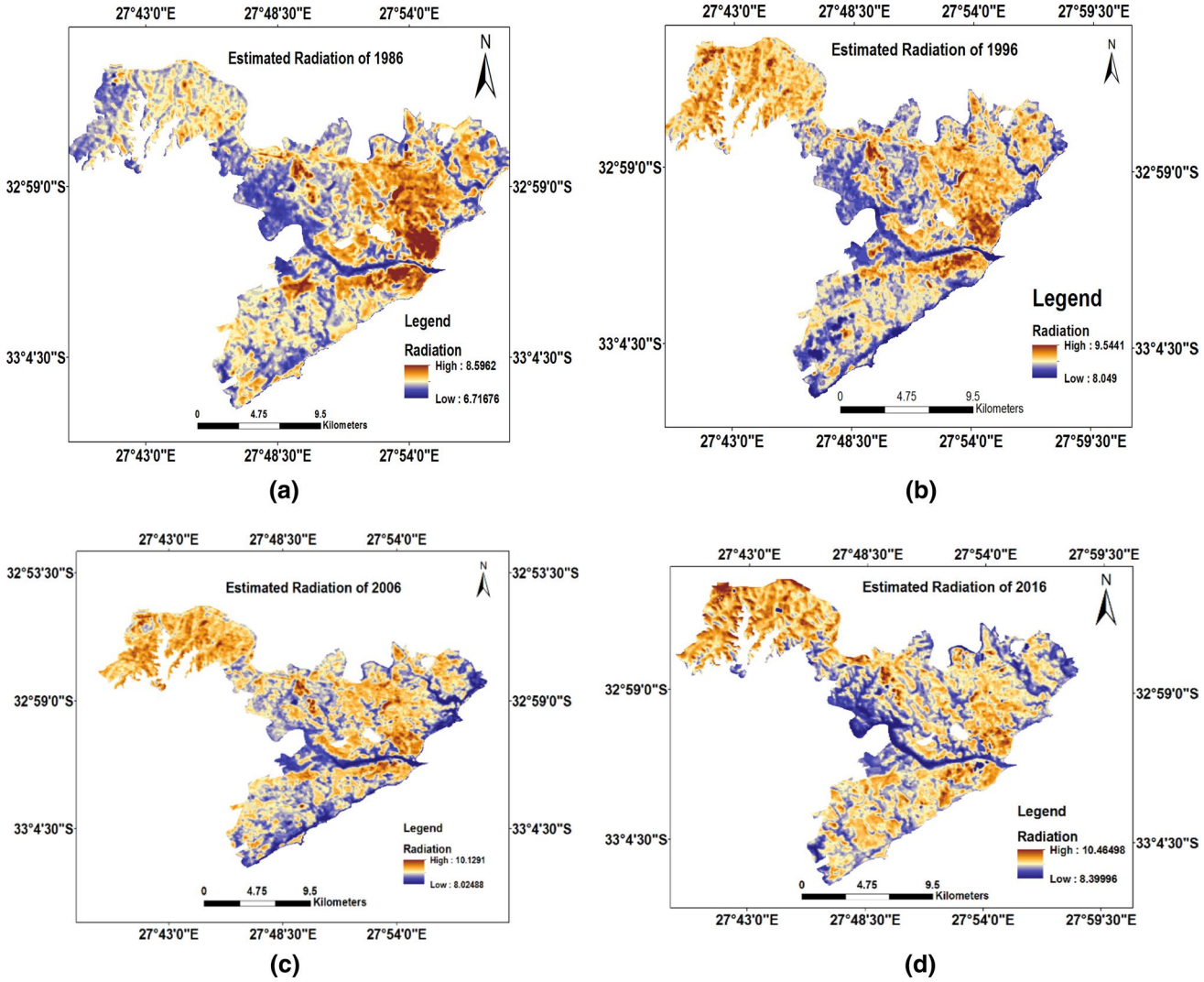

Fig. 5 Estimated radiation of East London between 1986 and 2016; **a** 1986, **b** 1996, **c** 2006, and **d** 2016

Table 4 Global solar radiation index threshold. *Source*: WHO (2012)

Threshold	Global solar radiation index risk level	Health effect
1–2	Low UV exposure	Normal
3–4	Moderate exposure	Fatigue possible with prolonged exposure
5–6	High exposure	Heat cramps, heat exhaustion with prolonged exposure
7–8	Very high exposure	Heat stroke and skin disease with prolonged exposure
> 9	Extreme exposure	Skin cancer, cardiovascular disease, heart stroke, and heat stroke

of ultraviolet reaching the surface varies in the daytime, it reaches extreme level, when there is no cloudy or overcast cover, around afternoon when there is sun. It is universally presented as a forecast of the highest amount of skin-threat solar radiation and is anticipated to reach the earth's surface at solar noon. The estimations of the index extend from zero upward, and the higher the index number, the more likelihood the probability of human health exposure to ultraviolet solar radiation, and the less time it takes for harm to happen (WHO 2003).

The analysis of surface radiation using GIS and remote sensing approach has shown that there is a variation of

solar radiation across the study area; using the global solar radiation index, it shows that East London area residents may be at risk with a prolonged exposure to the ultraviolet radiation from the sun (Williamson et al. 2014; Nakamura et al. 2015).

Conclusion and recommendation

For the past 3 decades, the East London area has undergone a dramatic transformation in the natural land features, resulting in vegetation loss and other land surface characteristics alteration. The analysis of land features using Landsat images to investigate features for a period of 30 years between 1986 and 2016 (1986, 1996, 2006, and 2016) utilizes supervised image classification techniques.

This study used the utilization of vegetation, built-up, water body, open surface, and beaches or shorelines division estimated from a spectral mixture grouping or classification as an indicator for the purpose of comparison. The outcomes revealed that the vegetation fraction gives a more grounded negative connection with LST for all land features at all levels, while built-up area and open surface give positive relationship of LST between 1986 and 2016. The LST pattern fluctuates with years, but yields the highest value around the built-up area followed by open surface. These discoveries propose that the areal measure of vegetation plenitude has a more direct correspondence with the radiative, thermal characteristics, and moisture attributes of the surface that control or influence LST. This research also reveals that the major land features that were used in the study area are vegetation.

Furthermore, surface thermal characteristics of the study area have significant health impacts using global solar radiation index. The global solar radiation index provides an easy measure of the solar UV radiation level at the earth's surface and thereby the potential impacts on human health such as heart disease and skin damage. From the analysis, it was revealed that between 1986 and 2016, the surface radiation varies from 6 upward—the higher the index value the more the potential for damage to the human health, and the less time it takes for harm to happen. Defensive measures should be taken for UV index threshold value of 4 and above.

Given the large public health burden of human, further investigation is needed in established case-specific causes. Thus, the present study illustrates that remote sensing and GIS are essential technologies for temporal analysis and quantification of a spatial phenomenon which is otherwise not possible to attempt with conventional mapping methods. Change detection is made easy with this technique in lesser time, at a low cost with better accuracy. This study also epitomises the significance of remote sensing climate variability studies.

Acknowledgements Authors would like to thank the US Geological Survey (USGS) for providing satellite imageries and University of Fort Hare, Alice, South Africa for creating an enabling environment for research.

Authors' contributions Orimoloye conducted the analysis and prepared the manuscript. Mazinyo and Nel supervised the research and Kalumba helped to proofread and gave his expertise idea about the work. All authors read and approved the final manuscript.

Compliance with ethical standards

Conflict of interest The authors declare that they have no competing interests.

References

Adefisan EA, Bayo AS, Ropo OI (2015) Application of geo-spatial technology in identifying areas vulnerable to flooding in ibadan metropolis. J Environ Earth Sci 5(14):153–166

Adeola AM, Botai JO, Rautenbach CD, Kalumba AM, Tsela PL, Adisa OM et al (2017) Landsat satellite derived environmental metric for mapping mosquitoes breeding habitats in the Nkomazi municipality, Mpumalanga Province, South Africa. South African Geographical Journal = Suid-Afrikaanse Geografiese Tydskrif 99(1):14–28

Balk SJ (2011) Ultraviolet radiation: a hazard to children and adolescents. Pediatrics 127(3):e791–e817

Bind MA, Zanobetti A, Gasparrini A, Peters A, Coull B, Baccarelli A, Schwartz J (2014) Effects of temperature and relative humidity on DNA methylation. Epidemiology (Cambridge, Mass.) 25(4):561

Carlson TN, Ripley DA (1997) On the relation between NDVI, fractional vegetation cover, and leaf area index. Remote sens Environ 62(3):241–252

Chander C, Markham H (2003) Revised Landsat-5 TM radio- metric calibration procedures and post-calibration dynamic ranges. IEEE Trans Geosci Remote 41:2674–2677

Conlon K, Monaghan A, Hayden M, Wilhelmi O (2016) Potential impacts of future warming and land use changes on intra-urban heat exposure in Houston, Texas. PLoS One 11(2):e0148890

Dai H, Zhang X, Hu Z (2017) Urbanization-induced land use and cover changes in Xuzhou, Jiangsu Province since the Mid-1990s. Geosci Res 2(3):172–179

Das D, Bakal JA, Westerhout CM, Hernandez AF, O'Connor CM, Atar D, Ezekowitz JA (2014) The association between meteorological events and acute heart failure: new insights from ASCEND-HF. Int J Cardiol 177(3):819–824

Fitchett JM, Robinson D, Hoogendoorn G (2017) Climate suitability for tourism in South Africa. J Sustain Tour 25(6):851–867

Hall R (2004) A political economy of land reform in South Africa. Rev Afr Polit Econ 31(100):213–227

Hall R (2007) Transforming rural South Africa? Taking stock of land reform. In: Ntsebeza L, Hall R (eds) The land question in South Africa. HSRC press, Cape Town, pp 87–106

Han J, Meng X, Zhou X, Yi B, Liu M, Xiang WN (2017) A long-term analysis of urbanization process, landscape change, and carbon sources and sinks: a case study in China's Yangtze River Delta region. J Clean Prod 141:1040–1050

Howard L (1833) The climate of London, vol I–III. Harvey and Dorton, London

Hu X, Zhou W, Qian Y, Yu W (2017) Urban expansion and local land-cover change both significantly contribute to urban warming,

but their relative importance changes over time. Landsc Ecol 32(4):763–780
Ige SO, Ajayi VO, Adeyeri OE, Oyekan KSA (2017) Assessing remotely sensed temperature humidity index as human comfort indicator relative to landuse landcover change in Abuja, Nigeria. Spat Inf Res 25(4):523–533
Intergovernmental Panel on Climate Change (2014) Climate change 2014—impacts, adaptation and vulnerability: regional aspects. Cambridge University Press, Cambridge
Kamusoko C (2017) Importance of remote sensing and land change modeling for urbanization studies. In: Urban development in Asia and Africa. Springer, Singapore, pp 3–10
Kruger AC, Shongwe S (2004) Temperature trends in South Africa: 1960–2003. Int J Climatol 24(15):1929–1945
Lahiff E, Cousins B (2005) Smallholder agriculture and land reform in South Africa. IDS Bull 36(2):127–131
Liu T, Yang X (2015) Monitoring land changes in an urban area using satellite imagery, GIS and landscape metrics. Appl Geogr 56:42–54
Lo CP, Quattrochi DA (2003) Land-use and land-cover change, urban heat island phenomenon, and health implications. Photogramm Eng Remote Sens 69(9):1053–1063
Mahmood R, Pielke RA, Hubbard KG, Niyogi D, Dirmeyer PA, McAlpine C et al (2014) Land cover changes and their biogeophysical effects on climate. Int J Climatol 34(4):929–953
Mather C, Greenberg S (2003) Market liberalisation in post-apartheid South Africa: the restructuring of citrus exports after' deregulation'. J South Afr Stud 29(2):393–412
Nakamura T, Yoshino H, Yamaguchi M, Tsujiguchi T, Chiba M, Hosoda M (2015) Report on the 1st Educational Symposium on RADIATION AND HEALTH by Young Scientists (ESRAH2014). Radiat Emerg Med 4:58–62
Oke TR (1978) Boundary layer climates. Methuen & Co., London
Onamuti OY, Okogbue EC, Orimoloye IR (2017) Remote sensing appraisal of Lake Chad shrinkage connotes severe impacts on green economics and socio-economics of the catchment area. R Soc Open Sci 4(11):171120
Pan Y, Zhai M, Lin L, Lin Y, Cai J, Deng JS, Wang K (2016) Characterizing the spatiotemporal evolutions and impact of rapid urbanization on island sustainable development. Habitat Int 53:215–227
Parker DE (2010) Urban heat island effects on estimates of observed climate change. Wiley Interdiscip Rev Clim Change 1(1):123–133
Peng SS, Piao S, Zeng Z, Ciais P, Zhou L, Li LZ, Zeng H (2014) Afforestation in China cools local land surface temperature. Proc Natl Acad Sci 111(8):2915–2919
Piao S, Yin G, Tan J, Cheng L, Huang M, Li Y, Poulter B (2015) Detection and attribution of vegetation greening trend in China over the last 30 years. Glob Change Biol 21(4):1601–1609
Repacholi MH (2000) Global solar UV index. Radiat Prot Dosim 91(1–3):307–311
Ropo OI, Perez MS, Werner N, Enoch TI (2017) Climate variability and heat stress index have increasing potential III-health and environmental impacts in the East London, South Africa. Int J Appl Eng Res 12(17):6910–6918
Roy DP, Kovalskyy V, Zhang HK, Vermote EF, Yan L, Kumar SS, Egorov A (2016) Characterization of Landsat-7 to Landsat-8 reflective wavelength and normalized difference vegetation index continuity. Remote Sens Environ 185:57–70
Shalaby A, Tateishi R (2007) Remote sensing and GIS for mapping and monitoring land cover and land-use changes in the Northwestern coastal zone of Egypt. Appl Geogr 27(1):28–41
Stephen H, Iortyom ET, Ropo OI, Daniel DP (2017) Analysis of the physical growth and expansion of Makurdi town using remote sensing and GIS techniques. Imp J Interdiscip Res 3(7):821–827
Streutker DR (2003) Satellite-measured growth of the urban heat island of Houston, Texas. Remote Sens Environ 85(3):282–289
Tewkesbury AP, Comber AJ, Tate NJ, Lamb A, Fisher PF (2015) A critical synthesis of remotely sensed optical image change detection techniques. Remote Sens Environ 160:1–14
Tursilowati L, Djundjunan JD (2007) Use of remote sensing and GIS to compute temperature humidity index as human comfort indicator relate with land use-land cover change (LULC) in Surabaya. In: Proceedings of the 73rd international symposium on sustainable Humanosphere, Bandung, Indonesia, pp 22–25
Wang C, Myint SW, Wang Z, Song J (2016) Spatio-temporal modeling of the urban heat island in the Phoenix metropolitan area: land use change implications. Remote Sens 8(3):185
Wang X, Guo W, Qiu B, Liu Y, Sun J, Ding A (2017a) Quantifying the contribution of land use change to surface temperature in the lower reaches of the Yangtze River. Atmos Chem Phys 17(8):4989–4996
Wang H, Zhang Y, Tsou JY, Li Y (2017b) Surface urban heat island analysis of Shanghai (China) based on the change of land use and land cover. Sustainability 9(9):1538
Weng Q, Lu D, Schubring J (2004) Estimation of land surface temperature—vegetation abundance relationship for urban heat island studies. Remote Sens Environ 89(4):467–483
Wichmann J, Andersen ZJ, Ketzel M, Ellermann T, Loft S (2011) Apparent temperature and cause-specific mortality in Copenhagen, Denmark: a case-crossover analysis. Int J Environ Res Public Health 8(9):3712–3727
Wilker EH, Yeh G, Wellenius GA, Davis RB, Phillips RS, Mittleman MA (2012) Ambient temperature and biomarkers of heart failure: a repeated measures analysis. Environ Health Perspect 120(8):1083
Williams D (2009) Landsat-7 science data user's handbook, vol 186. National Aeronautics and Space Administration, Washington
Williamson CE, Zepp RG, Lucas RM, Madronich S, Austin AT, Ballaré CL, Robinson SA (2014) Solar ultraviolet radiation in a changing climate. Nat Clim Change 4(6):434–441
World Health Organization (2003) The world health report 2003: shaping the future. WHO, Geneva
World Health Organization (2012) World health day 2012: Ageing and health: toolkit for event organizers. WHO
Xu H, Hu X, Guan H, He G (2017) Development of a fine-scale discomfort index map and its application in measuring living environments using remotely-sensed thermal infrared imagery. Energy Build 150:598–607
Zhou G, Wei X, Chen X, Zhou P, Liu X, Xiao Y, Su Y (2015) Global pattern for the effect of climate and land cover on water yield. Nat Commun 6:5918